Developments in the Built Environment 19 (2024) 100506

Contents lists available at ScienceDirect

Developments in the Built Environment

journal homepage: www.sciencedirect.com/journal/developments-in-the-built-environment

A circular approach to stone wool: Alkali-activated lightweight aggregates

C.H. Koh *, Y. Luo, K. Schollbach, F. Gauvin, H.J.H. Brouwers

Department of the Built Environment Eindhoven University of Technology P. O. Box 513, 5600 MB Eindhoven the Netherlands

ARTICLE INFO

Keywords:
Circularity
Stone wool
Alkali-activated material
Insulation
Hydrothermal

ABSTRACT

This study investigates the high-value recycling of stone wool from construction and demolition waste into alkali-activated lightweight insulation aggregates, designed for ground cover insulation. Various proportions of milled and as-is stone wools are alkali-activated to produce aggregates. The aggregates demonstrate loose bulk densities ranging from 720 to 850 kg m^{-3} and dry thermal conductivity from 0.075 to 0.094 W $m^{-1}{\cdot}K^{-1}$, with moderate water sorption capacities. The fibre morphology of as-is stone wool influences rheology, introducing a greater number of pores or defects, which results in a decrease in mechanical strength. Hydrothermal simulations reveal that the floor assembly of the rehabilitated crawl space, partially filled with the fabricated aggregates, shows a reduction in water content and an increase in floor surface temperature. This observation suggests potential benefits for maintaining the structural integrity of buildings and enhancing occupant comfort.

1. Introduction

In accordance with the European Waste Framework Directive (Directive, 2008), efforts to enhance the reuse, recycling and recovery of non-hazardous construction and demolition waste (CDW) have been mandated, with a target of achieving a minimum recycling rate of 70 % by weight. The Netherlands currently recycles approximately 88% of CDW (Conde et al., 2022). However, despite these high recycling rates, the majority of recycled construction materials are downcycled or repurposed for backfilling. Specifically, recycled materials from CDW account for only about 8% of all construction materials used in new buildings, with the remainder primarily downcycled in infrastructural projects (Conde et al., 2022). This practice does not align with the objectives of the National Circular Economy Programme established by the Dutch government to meet the growing demand for products and raw materials (IenW, 2023).

One of the key areas within the circularity action plans is the development of sustainable insulation materials. The goal is to adhere to circular design principles, thereby minimizing the incineration and landfilling of insulation materials at the end of their lifecycle. Insulation materials make up a significant proportion of CDW, with approximately 8.8% and 8.6% being landfilled and incinerated, respectively (Conde et al., 2022). Among these materials, stone and glass wool collectively represent a significant share of the thermal insulation market in Europe, accounting for approximately 58% of the volume in 2014 (Pavel and Blagoeva, 2018). Furthermore, the projected volumes of mineral wool waste in Europe exceed 2.5 million tonnes per year (Väntsi and Kärki, 2014). Therefore, high-value recycling of mineral wool is essential for achieving circularity targets.

Mineral wool waste exhibits homogenous physical and chemical properties compared to many other mineral wastes, making it a valuable source of consistent secondary raw materials (Yliniemi et al., 2021). The literature has explored various recycling approaches, including the use of mineral wool waste as reinforcement in cement mortar, thereby replacing conventional sand and aggregates (Ramírez et al., 2019; Gebremariam et al., 2021). Additionally, lightweight aggregates produced from stone wool and glass wool through high-temperature sintering have shown potential (López-García et al., 2022). Mineral wools are pozzolanic, making them potential precursors for producing alkali-activated materials (Mastali et al., 2021; Pavlin et al., 2021; Kinnunen et al., 2016). However, the reutilization of mineral wool in alkali-activated lightweight aggregates is currently limited, and their performance as insulation material remains an area of ongoing research. This limitation could be attributed to the fibrous and light-density nature of mineral wool, which makes it challenging to process. Nevertheless, two studies on alkali-activating stone wool are worth mentioning. In one study, waste stone wool from fine processing and crushed final products were alkali-activated to create artificial aggregates used in geopolymer mortar (Klima et al., 2023). Another study focused on alkali-activating stone wool waste from greenhouses to develop plant substrate materials (Oliveira et al., 2024). Both studies demonstrate the potential for repurposing stone wool waste through

* Corresponding author
E-mail address: k.c.h.koh.chuen.hon@tue.nl (C.H. Koh).

https://doi.org/10.1016/j.dibe.2024.100506
Received 19 June 2024; Received in revised form 14 July 2024; Accepted 14 July 2024
Available online 17 July 2024

alkali-activation and granulation.

This study investigates the potential fabrication and application of lightweight aggregates derived from stone wool for crawl space rehabilitation in the Netherlands. Many residential properties built before the 1970s in the Netherlands feature cavity walls and crawl spaces that require retrofitting (RVO, 2020). Conventional methods, such as spraying polyurethane (PUR) foam beneath the floor, are commonly employed for crawl space rehabilitation (RVO, 2021). However, these methods require sufficient crawl space height (above 35 cm) for access. For crawl spaces with limited accessibility (less than 35 cm), alternative strategies are necessary (Centraal, 2024). The lightweight aggregates developed in this study could potentially be applied in such retrofitting strategies, helping to mitigate ground moisture evaporation (Kurnitski, 2000) and improve occupant comfort and health (Vijay et al., 2019).

The primary objective of this study is to utilize stone wool as a precursor for producing alkali-activated lightweight aggregates. These aggregates are intended for use as ground cover insulation material in crawl space rehabilitation projects. Stone wool will be milled and alkali-activated to form aggregates, with unmilled stone wool included to provide porous structures. The characteristics and performance of the manufactured aggregates are investigated and utilized to simulate the hygrothermal performance of rehabilitated crawl spaces under typical Dutch climate conditions.

2. Material and methodology

2.1. Material and fabrication

In this study, commercially sourced stone wool, procured from Rockwool B.V. (Germany), is used as the primary material, simulating mineral wool waste free of significant impurities from other CDW. The chemical composition of the stone wool is analysed using X-ray fluorescence spectrometry (XRF) (PANalytical Epsilon 3) with a milled sample, and its loss on ignition (LOI) is determined within the temperature range of 105–1000 °C, as presented in Table 1. The length of stone wool varies, with length-weighted diameters ranging between 2.4 and 5.3 μm (Nielsen et al., 2013). Sodium silicate solution (27.7% SiO_2, 8.4% Na_2O and 63.9% H_2O) and sodium hydroxide (NaOH) pellets are used as the alkali activator.

The overall production procedure and specimen composition are depicted in Fig. 1. Unmilled stone wool, characterized by a fibrous and voluminous structure, exhibits low workability and strength when used in its original form. The initially long stone wool fibres (Fig. 1a) undergo milling to produce a powder (Fig. 1b) using a ball mill (Planetary Mill Pulverisette 5). This milled stone wool serves as the solid precursor in the alkali-activated binder for this study. Additionally, as-is stone wool is incorporated into the mixture as a micro-fibre to enhance porosity and thermal insulation. Five distinct weight ratios of milled and as-is stone wool are prepared: 9.0, 6.1, 4.6, 3.5, and 2.8, denoted as M90, M86, M82, M78 and M74 respectively (refer to Fig. 1c). The workability of the paste deteriorates when the weight ratio decreases to 2.5 or lower. The alkali activator is synthesized in advance by blending sodium silicate solution, sodium hydroxide pellets, and additional water. The alkali activator formulation is established with a modulus of 1.8 and Na_2O concentration of 8%, based on a previous fly ash-based geopolymer formulation (Koh et al., 2024). The water-to-dry components ratio (dry sodium silicate, sodium hydroxide, milled stone wool and as-is stone wool) is set at 0.4. The mass ratio of liquid (alkali activator solution and water) to precursor (milled stone wool) is fixed at 72%.

Table 1
Chemical composition of raw material.

Oxides (%)	Stone Wool
SiO_2	38.11
Al_2O_3	23.18
CaO	16.82
MgO	8.91
Fe_2O_3	7.43
TiO_2	1.56
K_2O	0.74
MnO	0.28
SO_3	0.07
Cr_2O_3	0.07
V_2O_5	0.05
Other	0.64
LOI (1000°C)	2.14
Specific density ($kg{\cdot}m^{-3}$)	2800 ± 2

For the production process, milled stone wool and alkali activator solution are combined in a mixer and blended until a homogeneous paste is attained. Subsequently, as-is stone wool is added to the paste and thoroughly mixed until all fibres are coated. In this lab-scale manufacturing process, aggregates are shaped by placing the mixed material into spherical silicone moulds. For upscaling production, extrusion is suggested. The average diameter of the aggregates obtained is 2 ± 1 cm. The moulds containing aggregates are wrapped in plastic foil and cured in an oven at 60 °C for 24 h. Following curing, the aggregates are removed from the mould and subjected to further drying in an oven at 60 °C for an additional 12 h. Finally, the aggregates are retrieved from the oven for further characterization and assessment.

2.2. Characteristics assessment

Loose bulk density (ρ_{bulk}) of the aggregates is determined in accordance with standard EN1097-3 (CEN, 1998). Particle density ($\rho_{particle}$) is assessed using a helium pycnometer (Micromeritics AccuPyc II 1340) with a 10 cm^3 cup is used. The pycnometer has a reading accuracy of 0.03% and an additional 0.03% uncertainty related to the sample capacity. Porosity of the specimen is calculated from particle density and bulk density using the formula:

$$porosity = 1 - \frac{\rho_{bulk}}{\rho_{particle}} \quad (1)$$

Open porosity is directly measured from the aggregates, while total porosity is determined from the powder obtained from crushed and milled aggregates.

Mechanical property is assessed using a mechanical testing system (Instron 5967) equipped with a 5 kN load cell. Single crushing strength (σ) is calculated using the formula proposed by (Hiramatsu et al., 1965):

$$\sigma = \frac{2.8 * P}{\pi * d^2} \quad (2)$$

Where P represents the recorded failure load and d is the diameter of aggregate. An average value is computed from 10 aggregates per specimen group.

Thermal conductivity (λ) is determined utilizing the transient line source method with a thermal needle probe (AP Isomet model 2104). The probe has an accuracy of 5% of the reading plus 0.001 W $m^{-1}{\cdot}K^{-1}$. Measurements are taken at 20 ± 2 °C, with three readings obtained per specimen group. To ensure consistency in measurements, samples are filled into the same cylindrical container utilized to determine bulk density.

Hygroscopic sorption properties are evaluated following standard ISO 12571 (CEN, 2013a). Sorption isotherms are measured by the saturated salt solutions (SSS) method, covering specific relative humidity levels from 0% to 98%. Moisture uptake is monitored by weighing the samples at 24-h intervals using a digital balance until a constant mass is reached, defined as three successive weighings showing a mass loss change of less than 0.1%.

Water absorption is measured in accordance with standard EN1097-6 (CEN, 2013b). Samples are immersed in water in a pyknometer for 24 h, and the mass of the saturated and surface-dried aggregates is recorded.

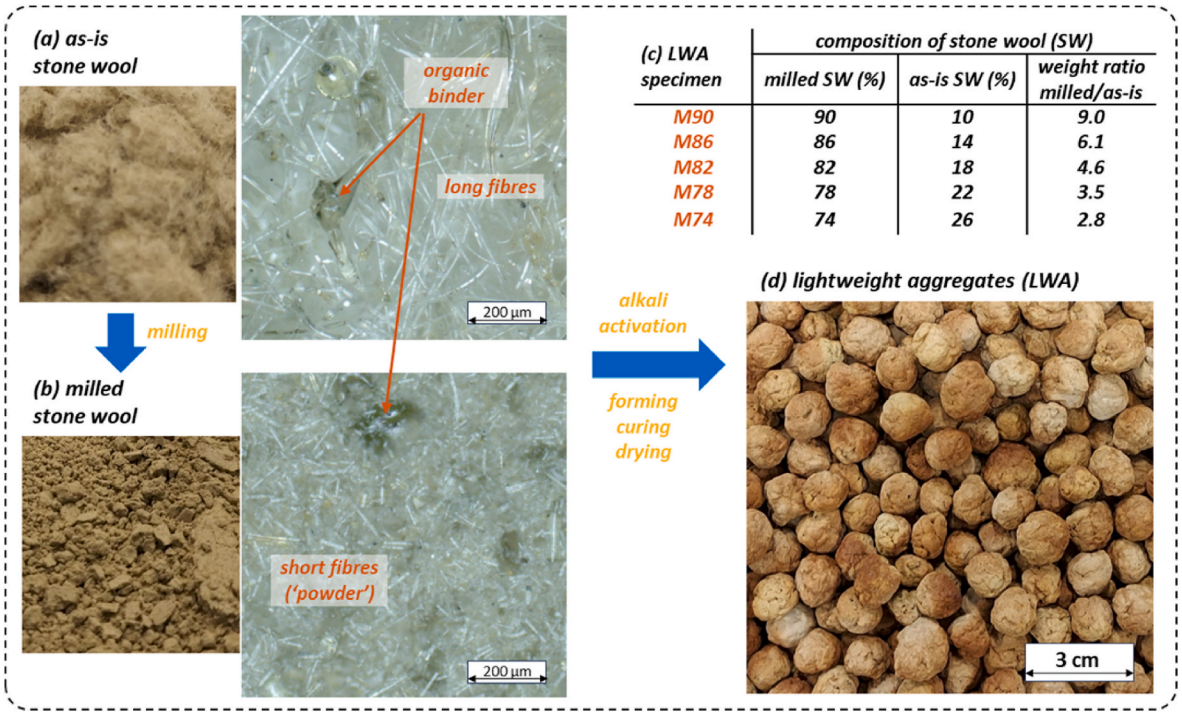

(c) LWA specimen	composition of stone wool (SW)		
	milled SW (%)	as-is SW (%)	weight ratio milled/as-is
M90	90	10	9.0
M86	86	14	6.1
M82	82	18	4.6
M78	78	22	3.5
M74	74	26	2.8

Fig. 1. (A) As-is stone wool, (b) milled stone wool, (c) specimen compositions, and (d) manufactured stone wool-based lightweight aggregates (LWA).

Microstructure analysis is performed through visual inspection using an optical microscope (ZEISS Axio Imager 2).

Thermogravimetric analysis (TGA) is conducted to assess mass loss or decomposition events with respect to temperature, utilizing a thermogravimetric analyser (TA Instruments TGA Q500). The heating process, starting from room temperature and continuing up to 1000 °C at a rate of 10 °C·min^{-1}, is carried out under a controlled nitrogen atmosphere with a constant flow rate of 60 ml min^{-1}.

Chemical composition analysis is performed using Fourier transform-infrared (FT-IR) spectroscopy coupled with an attenuated total reflection (ATR) attachment (PerkinElmer Frontier FT-IR). Spectra are collected over a wavenumber range of 4000 to 400 cm^{-1} at a resolution of 1 cm^{-1}.

Mineralogical composition is further characterized by X-ray diffraction (XRD), utilizing a Bruker D2 (Co tube, Kα1 1.7890 [Å] Kα2 1.7929 [Å], step size 0.02 2Theta, range 10–90 2Theta).

2.3. Building performance simulation

Heat, air and moisture (HAM) transport simulations and indoor climate analyses are conducted on a terraced housing unit with a narrow crawl space and cavity walls, based on a model established in a prior study (Koh et al., 2022). Specifically, the water content and temperature of the floor (wooden flooring and floor joist) above the crawl space are examined for the original unfilled crawl space and the crawl space filled with lightweight aggregates manufactured in this study. The software WUFI Plus is utilized to compute the heat and moisture balances within the room (WUFI, 2018) using the following equations:

$$\frac{\partial H}{\partial t} = \sum_j Q_{comp,j} + Q_{sol} + Q_{in} + Q_{vent} + Q_{HVAC} \quad (3)$$

and

$$\frac{\partial C}{\partial t} = \sum_j \dot{W}_{comp,j} + \dot{W}_{in} + \dot{W}_{vent} + \dot{W}_{HVAC} \quad (4)$$

Here, H (J) represents the overall enthalpy of the air in the simulated zone, C (kg) the overall moisture content of the air in the simulated zone, $Q_{comp,j}$ (W) the transmission heat flow over component j, Q_{sol} (W) the short-wave solar radiation leading directly to heating the inner air, Q_{in} (W) the convective heat sources in the room, Q_{vent} (W) the heat flow from ventilation, Q_{HVAC} (W) the convective heat flow from building ventilation systems, $\dot{W}_{comp,j}$ (kg·s^{-1}) the moisture flow between the inner wall surface j and room air, $\dot{W}_{in}$ (kg·s^{-1}) the moisture source in the room, $\dot{W}_{vent}$ (kg·s^{-1}) the moisture flow due to ventilation, and $\dot{W}_{HVAC}$ (kg·s^{-1}) the moisture flow due to building ventilation systems.

The building model encompasses dimensions of 5 × 8x2.8 m^3 per floor (width x depth x height) per housing unit, each featuring a floor area of 80 m^2 and an unheated attic, refer to Fig. 2a. An elevated wooden floor above sandy ground creates a narrow crawl space with a height of 30 cm (Fig. 2b), exhibiting an arbitrary air change rate of 10 h^{-1} with the outdoor environments. Two-floor assembly designs are considered: one with the original unfilled crawl space and another filled with a 20 cm thick layer of manufactured aggregates on the sandy ground, leaving only 10 cm of airspace. The effective thermal transmittance (U-value) of the floor assembly with the unfilled crawl space is 0.332 W m^{-2}·K^{-1}. Masonry walls with a 6 cm cavity filled with stone wool exhibit a U-value of 0.499 W m^{-2}·K^{-1}. Additional building components include a ceiling assembly with a U-value of 0.087 W m^{-2}·K^{-1} and glazing with a U-value of 0.8 W m^{-2}·K^{-1}.

Boundary conditions are established based on the outdoor climate of Eindhoven in the Netherlands, characterized by a temperate oceanic climate (Cfb) according to the Köppen climate classification. The annual air temperature and relative humidity profile (Crawley and Lawrie, 2023) are depicted in Fig. 2c. Two indoor scenarios are defined: one with a heating system maintaining an indoor temperature above 20 °C, and another without any heating system. Cooling systems, mechanical humidification, and dehumidification systems are excluded, as they are not commonly utilized in residential housing in the Netherlands. A steady airflow of 7 l s^{-1} per person is incorporated into the model. The indoor heat and moisture loads are based on the software's predefined four-person family household occupancy. The simulation is conducted for three years or until hygrothermal equilibrium within the building assemblies is reached.

The simulated results are further compared against another

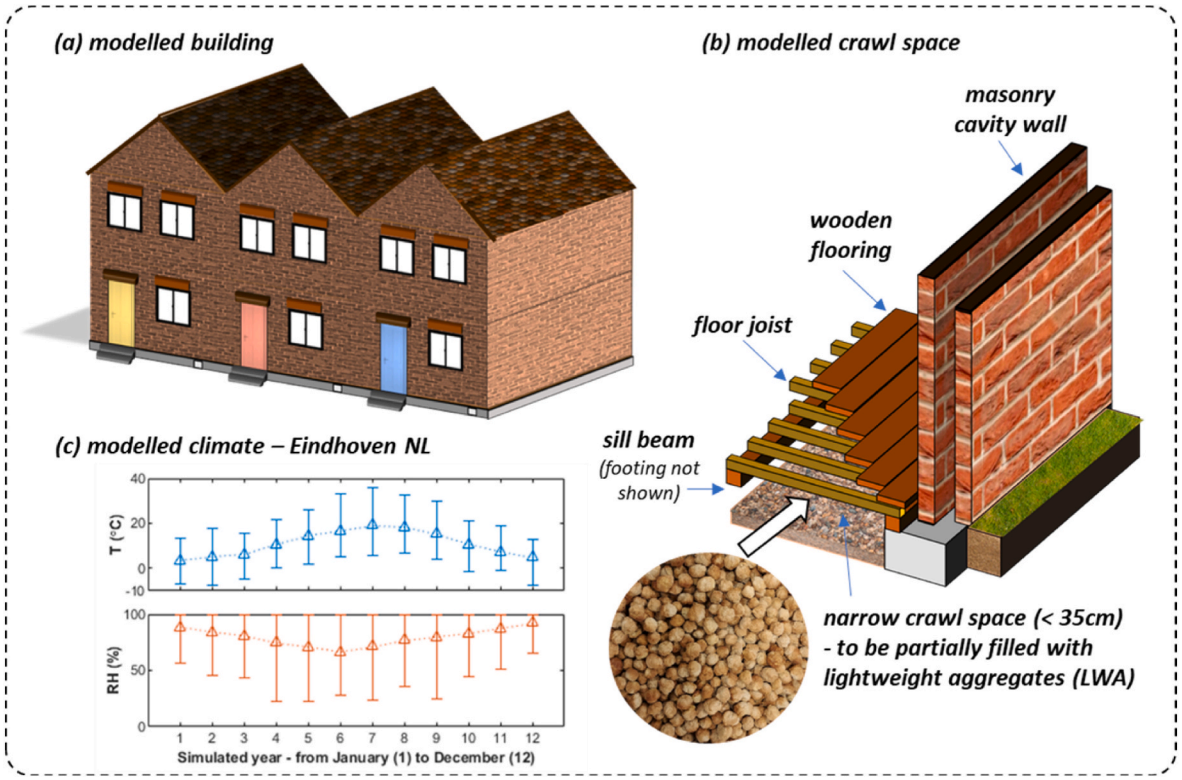

Fig. 2. (A) Building model, (b) crawl space design, and (c) exterior climates for simulation.

commonly applied insulation aggregate, namely expanded perlite aggregates (EPA). The main properties of the reference material are: bulk density of 147 kg m^{-3}, porosity of 0.94, thermal conductivity of 0.04 and 0.05 W $m^{-1}{\cdot}K^{-1}$ under dry and 60% relative humidity (RH) conditions, respectively, and moisture content of 1 %kg·kg^{-1} under 60% RH (WUFI Mateial Database).

3. Results and discussions

3.1. Characteristics assessment

In this study, an increase in the content of as-is stone wool results in a more porous aggregate structure, as demonstrated by the elevated porosity and reduced bulk density (Fig. 3a–b). The internal porosity of the aggregates primarily comprises interconnected and open pores, with

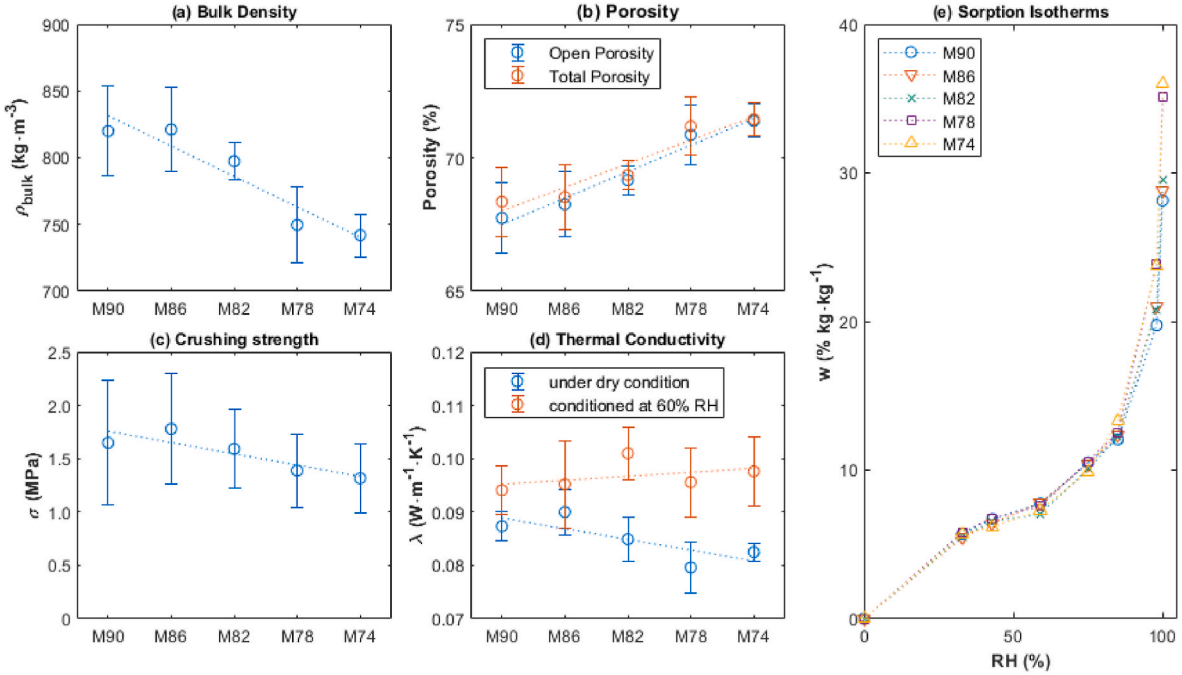

Fig. 3. (A) Bulk densities, (b) porosities, (c) crushing strength, (d) thermal conductivities, and (e) sorption isotherms of specimens.

closed pores constituting less than 1% of the sample porosity. The bulk densities range from 720 (M74) to 850 kg m^{-3} (M90), slightly lower than those reported for similar lightweight aggregates (LWA) derived from stone wool precursors, such as the 860 kg m^{-3} reported by (López-García et al., 2022). This reduction in weight primarily stems from the combination of as-is and milled stone wool used in this study. While the loose bulk density adheres to the 1200 kg m^{-3} limit defined for LWA (CEN, 2016), these aggregates display notably higher densities than conventional expanded perlite aggregates (EPA), which typically range from 30 to 150 kg m^{-3} (ISO, 2007). This suggests a higher anticipated thermal conductivity; however, it also provides greater thermal mass than EPA.

The individual aggregate crushing resistance ranges between 1.0 and 2.3 MPa (Fig. 3c). The highest strength is observed in the M86 specimen. The results show that the strength decreases as a higher percentage of as-is stone wool is incorporated. The incorporation of as-is stone wool can impact rheology due to its fibre morphology, introducing more pores or defects. However, the overall strength is notably lower than that reported for other stone wool-based LWA, such as 8.8 MPa reported by (López-García et al., 2022) and 7.0 MPa by (Klima et al., 2023). It is important to note that the higher strengths achieved in these studies are attributed to additional high-temperature sintering following the curing process. For loose-fill insulation applications in crawl spaces, crushing resistance is primarily necessary for the handling and installation of the material. Therefore, a comparable lower strength can be tolerated, and more importantly, lower energy manufacturing is achieved.

The dry thermal conductivity of the samples falls within the range of 0.075 and 0.094 W $m^{-1}{\cdot}K^{-1}$ (Fig. 3d). A decrease in thermal conductivity is observed with increasing as-is stone wool contents, aligning directly with the higher porosity evident in the aggregates. The greater volume of air voids within the aggregates results in reduced thermal conductivity. This range is consistent with other alkali-activated aggregates, as reported between 0.079 and 0.087 W $m^{-1}{\cdot}K^{-1}$ by (Zorić et al., 2012). However, the thermal conductivity is higher than that of typical EPA, which typically ranges from 0.04 to 0.05 W $m^{-1}{\cdot}K^{-1}$ (ISO, 2007), owing to their lower density. Under 60% relative humidity (RH) conditions, the thermal conductivity increases. Conversely, when compared against as-is stone wool contents, the thermal conductivity exhibits a slight increase with higher as-is stone wool contents. The heightened presence of open pores results in increased water content within the aggregate, subsequently elevating its effective thermal conductivity under high RH conditions. This suggests that further increases in as-is stone wool contents to achieve a more porous structure may compromise insulation performance in humid environments.

The moisture adsorption of the samples shows no significant difference up to 85% RH, with water contents measuring at 7 and 11 % kg·kg^{-1} under 60% and 80% RH respectively (Fig. 3e). The influence of as-is stone wool contents becomes more pronounced regarding water absorption capability. Water contents up to 36 %kg·kg^{-1} are measured in samples M74 and M78, while approximately 28 %kg·kg^{-1} is observed in samples M82, M86 and M90 under fully saturated conditions. This observation suggests the formation of larger pores when as-is stone wool content exceeds 22% in composition. It also implies that the thermal conductivity of aggregates with higher as-is stone wool contents will increase significantly under higher RH or when in contact with water, which is undesirable, especially when they are directly in contact with the ground. For comparison, water content for EPA is typically around 1 and 2 %kg·kg^{-1} under 60% and 80% RH respectively (ISO, 2007), although water absorption can reach as high as 71 %kg·kg^{-1} (Celik et al., 2013) due to the presence of large pores.

Pores are readily observable on the manufactured samples, as depicted in Fig. 4. The as-is stone wool entraps air bubbles during the gel formation process, particularly in areas where wool is aggregated. This phenomenon leads to the formation of larger pores and defects within the matrix. Smaller pores are also discernible and randomly distributed within the binder gel. The internal structure exhibits a notable degree of inhomogeneity due to the random distribution of as-is stone wool and the lab-scale fabrication process.

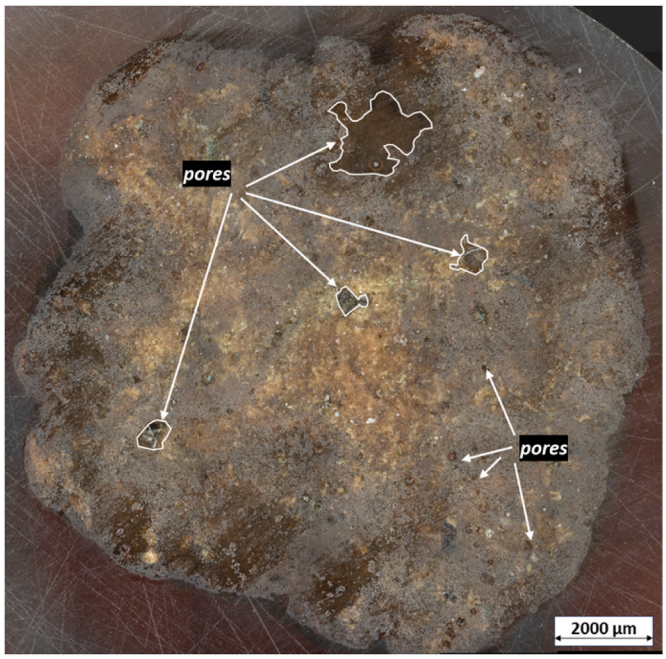

Fig. 4. Microscope images of samples M82 showing pores.

Fig. 5a depicts the results of thermogravimetric (TG) analysis conducted on the crushed powder extracted from the aggregates. The initial derivative thermogravimetry (DTG) peak emerges within the temperature range of 100–300 °C, signifying the release of physically and chemically bound water inherent in the aluminosilicate gel structure (Luo and Yu, 2024). A subtle shift of the peak towards higher temperatures is observed with increased milled stone wool incorporation, transitioning from 179 °C for M74/M78 to 185 °C for M86/M90. This shift is attributed to the rapid dissolution rate of milled stone wool compared to as-is stone wool, leading to an enhanced gel formation with more tightly bonded water, thus corroborating the observed trends in crushing strength. The original organic binder present in stone wool (Fig. 1) undergoes decomposition within the range of 300–500 °C (Chen et al., 2023; Kizinievič et al., 2014). When exposed to the alkaline solution, the organic binder decomposes and releases ammonia, potentially increasing the porosity of the binder (Luo and Yu, 2024). Additionally, the DTG peak at 700 °C corresponds to the decomposition of carbonates (Luo and Yu, 2024). However, within the same temperature range, an exothermic peak at 700 °C is notable, particularly in raw stone wool, which may signify the devitrification of wool and subsequent formation of crystalline phases (Ramírez et al., 2018; Siligardi et al., 2017). A similar exothermic peak is also discernible in the aggregates, especially those with higher as-is stone wool content such as M74.

Fig. 5b illustrates the Fourier transform-infrared (FT-IR) spectroscopy analysis on both the aggregates and raw stone wool. The primary peak at broad bands around 900 cm^{-1} on raw stone wool corresponds to the asymmetric stretching vibration modes of *Si–O*-T bonds (T = tetrahedral Si or Al) (Pavlin et al., 2021). Upon alkali activation, the bands in the aggregates are shifted and centred at or around 980 cm^{-1}. This shift primarily reflects changes in the polymerization degree of *Si–O*-T crosslinking. In this investigation, an increase in milled stone wool leads to the shifting of the main *Si–O*-T band from 960 cm^{-1} to 980 cm^{-1}, indicating a higher polymerization degree with milled stone wool, consistent with the TG measurement. The humps at 1400 cm^{-1} and 1460 cm^{-1} are attributed to the presence of various carbonates (Luo and Yu, 2024). Small peaks at 1640 cm^{-1}, attributed to OH groups (Gao

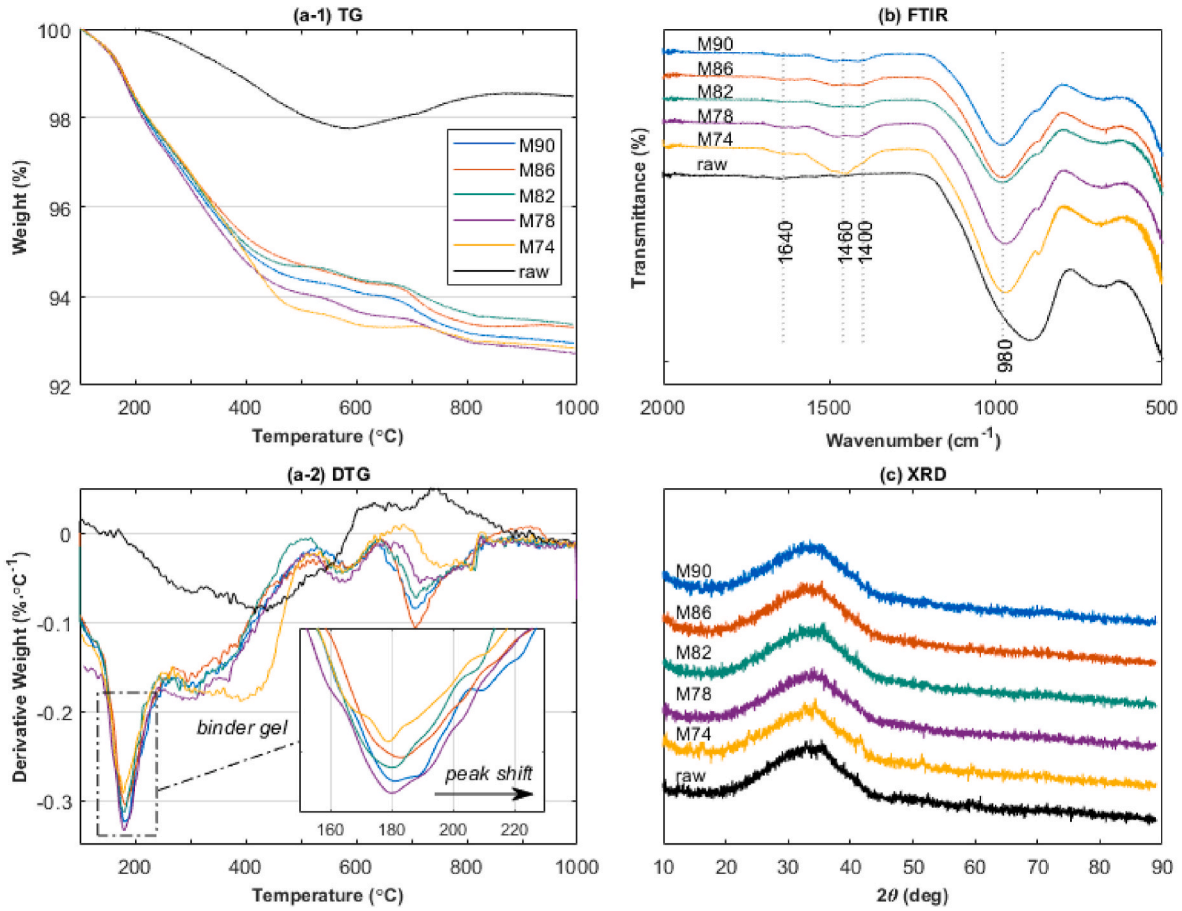

Fig. 5. (A) TG/DTG, (b) FTIR, and (c) XRD patterns of specimens and raw material.

et al., 2015), originating from chemically bound water in the gel, are also observed.

Raw stone wool primarily exhibits an amorphous structure, attributable to the rapid cooling during the manufacturing process (Kinnunen et al., 2016; Chen et al., 2023; Chen et al., 2019), as confirmed by X-ray diffraction (XRD) analysis (Fig. 5c), wherein no discernible peaks are evident, but rather a broad halo around 30° 2θ. Similarly, the alkali-activated aggregates retain an amorphous nature without any crystalline phase formation, which is consistent with the findings reported by (Pavlin et al., 2021).

Based on the crushing strength results, specimen M86 is selected for further hygrothermal performance simulation as insulation aggregates for crawl space rehabilitation. The aggregates have a measured bulk density of 821 kg m^{-3}, open porosity of 68%, dry thermal conductivity of 0.090 W m^{-1}·K^{-1}, heat capacity of 800 J kg^{-1}·K^{-1}, and sorption isotherms as shown in Fig. 3e. The aggregates are assumed to be vapour-diffusive, with a water vapour diffusion resistance factor of 2. Additionally, the aggregates are assumed to exhibit the same liquid transport properties as sands to account for additional capillary liquid transport during the hygrothermal simulation.

3.2. Building performance simulation

The water content profiles of the floor assembly, comprising the wooden flooring exposed to the indoor environment and the floor joist exposed to the crawl space, are depicted in Fig. 6. Both heated and unheated building scenarios are considered for comparison. In cold climates, building design typically incorporates a heating system to maintain an indoor temperature of approximately 20 °C or higher, thereby preventing damage from ground frost, structural wetting, mould formation, and other moisture-related issues (Viljanen et al., 1999). These distinct trends in water content within the floor assembly are discernible in the simulated profiles presented in Fig. 6.

In both heated and unheated scenarios, a reduction in water content is observed in the floor assembly of the rehabilitated crawl space partially filled with M86 aggregates, compared to the original construction with an empty crawl space. The reduction is more pronounced in the floor joist exposed to the crawl space, with reductions of up to 2.9% for heated buildings and up to 2.7% for unheated buildings (Fig. 6b). Conversely, for the flooring exposed to the indoor environment, reductions of approximately 1.2% and 0.5% are observed for heated and unheated buildings, respectively (Fig. 6a).

The moisture reduction profiles of M86 aggregates and conventional EPA used as filling aggregates for floor rehabilitation follow a similar trend. However, conventional EPA performs slightly better than M86 aggregates, providing up to an additional 0.2% moisture reduction in wooden flooring and an additional 0.4% moisture reduction in wooden floor joists. This difference is mainly due to the lower moisture sorption capacity of conventional EPA compared to the M86 aggregates manufactured in this study.

Despite the relatively small reduction in moisture content, these improvements within the floor assembly offer potential benefits in mitigating structural damage, mould proliferation, or other health and safety hazards associated with undesirable levels of moisture content (Vijay et al., 2019). The simulated results in this study are consistent with previous research on measured and simulated moisture conditions in outdoor air-ventilated crawl spaces with ground cover, showing a reduction in relative humidity in the rehabilitated crawl space (Kurnitski and Matilainen, 2000).

The effective thermal transmittance (U-value) of the rehabilitated

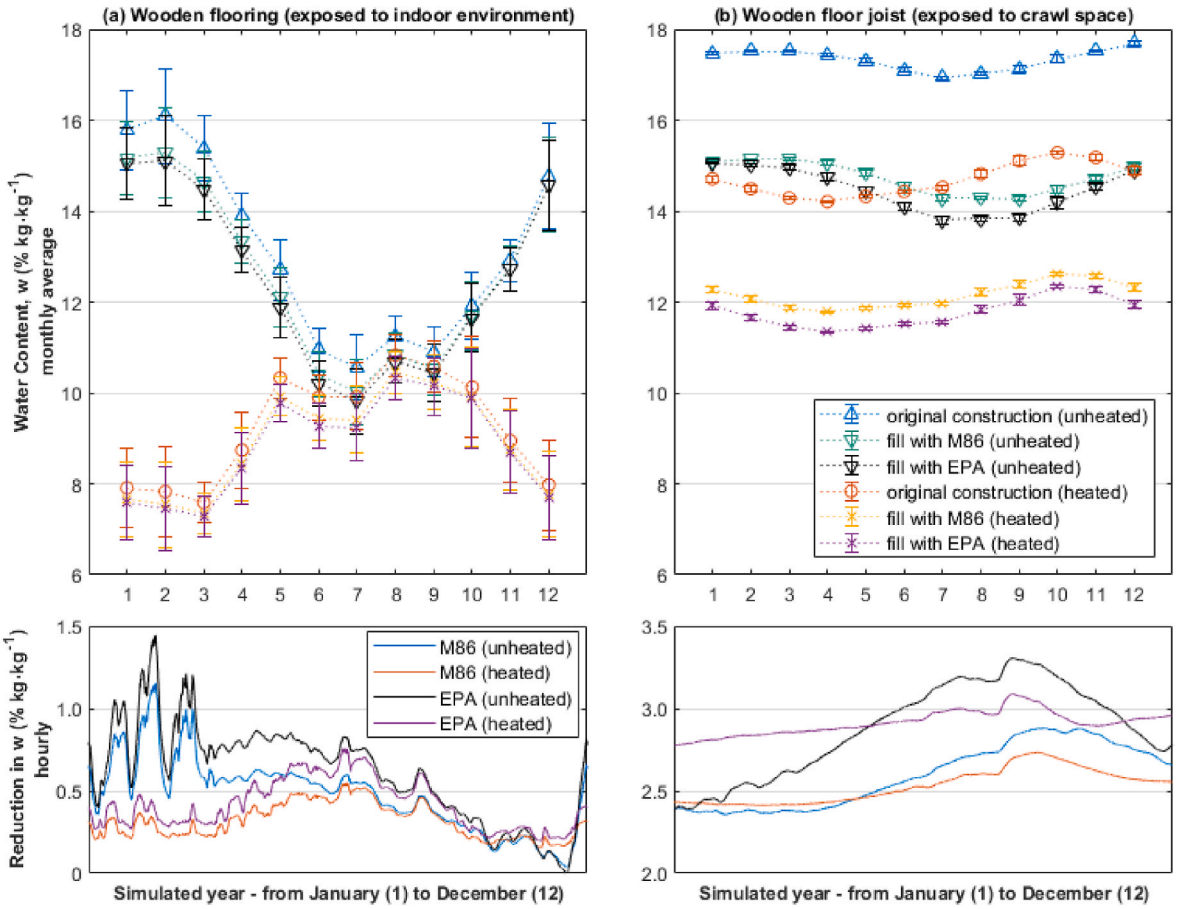

Fig. 6. Average water content in the floor assembly: (a) wooden flooring that is exposed to the indoor environment and (b) wooden floor joist that is exposed to crawl space.

floor assembly, filled with M86 aggregates, decreases from 0.332 W $m^{-2}{\cdot}K^{-1}$ to 0.191 W $m^{-2}{\cdot}K^{-1}$, compared to 0.121 W $m^{-2}{\cdot}K^{-1}$ when filled with EPA. For energy retrofitting of a ventilated crawl space, the most effective approach involves adding an insulation layer beneath the floor if sufficient crawl space height is available. Consequently, only a minor increase in floor temperature is observed when aggregates are placed on the ground in the crawl space, as illustrated in Fig. 7.

During the winter period, temperature increments of up to 0.2 °C and 0.4 °C are noted for heated and unheated buildings, respectively, when applying M86 aggregates. Conversely, using conventional EPA as ground cover insulation offers an additional 0.1 °C increment due to its lower thermal conductivity. For heated buildings, ground cover with M86 aggregates translates into an energy saving of 5.4% based on simulation results, reducing from 5992 to 5669 kWh after rehabilitation. This is slightly lower than the EPA case, which provides a 7.0% energy saving.

Interestingly, an undesirable decrease in temperature is observed in unheated buildings during the early winter period. This phenomenon is attributed to reduced access to ground heat, which could be more pronounced with materials of lower thermal conductivity or thermal mass, such as expanded perlite aggregates. However, it is important to note that this phenomenon is limited to unheated buildings.

4. Conclusion

The properties of the fabricated stone wool-based aggregates are determined by the ratio of milled stone wool to as-is stone wool in their compositions. It has been observed that the fibre morphology of as-is stone wool influences rheology, introducing a greater number of pores or defects, which results in a decrease in mechanical strength. As the proportion of as-is stone wool increases from 10% to 26% in the stone wool mixture, there is a corresponding increase in the porosity of the specimens from 67% to 72%. These porous structures exhibit a thermal conductivity ranging from 0.075 to 0.094 W $m^{-1}{\cdot}K^{-1}$ under dry conditions. However, under humid conditions, aggregates with higher porosity demonstrate an increase in thermal conductivity, which can be attributed to their elevated moisture adsorption and water absorption capacity. When compared to conventional expanded perlite aggregates (EPA), the fabricated aggregates exhibit certain disadvantages such as higher density, thermal conductivity, and moisture adsorption capacity. However, they offer advantages such as lower water absorption and higher thermal mass.

In the hydrothermal simulation involving the use of stone wool-based aggregates for crawl space rehabilitation, a notable reduction in water content and an increase in floor surface temperature are observed in the floor assembly of the rehabilitated crawl space partially filled with aggregates, compared to the original construction with an empty crawl space. This decrease in water content within the floor assembly offers potential advantages for maintaining the structural integrity of buildings and mitigating adverse impacts on occupant comfort and health. Furthermore, there is potential for a 5.4% reduction in heating energy consumption after rehabilitation.

The findings of this study suggest that stone wool-based aggregates provide a high-value recycling option suitable for crawl space retrofitting applications. These aggregates and their potential applications represent sustainable construction practices, contributing to the circular economy by repurposing insulation waste materials into valuable building insulation components. Future research should focus on the

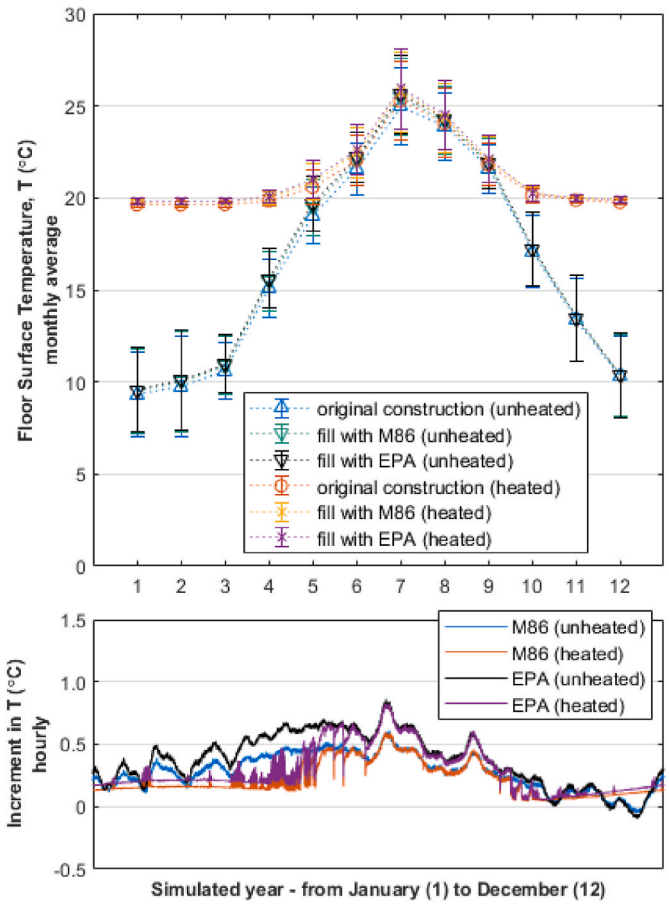

Fig. 7. Average floor surface temperature.

durability of these aggregates when exposed to water and freeze-thaw cycles, their leaching behaviour, composition design, manufacturing optimization, and conducting a full life cycle assessment and life cycle costing to ensure practical implementation.

CRediT authorship contribution statement

C.H. Koh: Writing – original draft, Software, Methodology, Investigation, Formal analysis, Conceptualization. **Y. Luo:** Methodology, Conceptualization. **K. Schollbach:** Writing – review & editing, Supervision. **F. Gauvin:** Writing – review & editing, Supervision. **H.J.H. Brouwers:** Writing – review & editing, Supervision.

Declaration of competing interest

The authors declare that they have no known competing financial interests or personal relationships that could have appeared to influence the work reported in this paper.

Data availability

Data will be made available on request.

References

98/EC"On waste and repealing certain Directives," European Parliament and Council. http://data.europa.eu/eli/dir/2008/98/2018-07-05.
Celik, A.G., Kilic, A.M., Cakal, G.O., 2013. Expanded perlite aggregate characterization for use as a lightweight construction raw material. Physicochem. Probl. Miner. Process. 29 (2), 689–700. https://doi.org/10.5277/ppmp130227.
CEN, 1998. EN 1097-3 Test for Mechanical and Physical Properties of Aggregates - Part 3: Determination of Loose Bulk Density and Voids.
CEN, 2013a. ISO 12571 Hygrothermal Performance of Building Materials and Products - Determination of Hygroscopic Sorption Properties.
CEN, 2013b. EN 1096-6 Test for Mechanical and Physical Properties of Aggregates - Part 6: Determination of Particle Density and Water Absoption. CEN.
CEN, 2016. EN 13055 LighCtweight Aggregates. CEN.
Centraal, Milieu, 2024. Geen of lage kruipruimte, wat nu? [Online]. Available: https://www.milieucentraal.nl/energie-besparen/isoleren-en-besparen/vloerisolatie/#geen-of-lage-kruipruimte-wat-nu.
Chen, Z., Wang, H., Ji, R., Liu, L., Cheeseman, C., Wang, X., 2019. Reuse of mineral wool waste and recycled glass in ceramic foams. Ceram. Int. 45 (12), 15057–15064. https://doi.org/10.1016/j.ceramint.2019.04.242.
Chen, C., Wang, X., Wang, Y., Jiu, S., Chen, Y., 2023. Effect of rock-wool waste on physical, mechanical, and microscopic properties of nonburn solid bricks. Construct. Build. Mater. 392, 131805 https://doi.org/10.1016/j.conbuildmat.2023.131805.
Conde, A., Sutherland, A.B., Fraser, M., Roemers, G., Sosa, L., Rohmer, M., 2022. The Circularity Gap Report: Built Enviroment. Circle Economy, the Netherlands.
Crawley, D., Lawrie, L., 2023. Climate.OneBuilding.Org [Online]. Available: https://climate.onebuilding.org/default.html. (Accessed 25 March 2022).
Gao, X., Yu, Q., Brouwers, H.J.H., 2015. Properties of alkali activated slag–fly ash blends with limestone addition. Cement Concr. Compos. 59, 119–128. https://doi.org/10.1016/j.cemconcomp.2015.01.007.
Gebremariam, A.T., Vahidi, A., Maio, F.D., Moreno-Juez, J., Vegas-Ramiro, I., Łagosz, A., Mróz, R., Rem, P., 2021. Comprehensive study on the most sustainable concrete design made of recycled concrete, glass and mineral wool from C&D wastes. Construct. Build. Mater. 273, 121697 https://doi.org/10.1016/j.conbuildmat.2020.121697.
Hiramatsu, Y., Oka, Y., Kiyama, H., 1965. Rapid determination of the tensile strength of rocks with irregular test pieces. J. Min. Metall. Inst. Jpn. 81 (932), 1024–1030. https://doi.org/10.2473/shigentosozai1953.81.932_1024.
IenW, 2023. "National Circular Economy Programme 2023-2030," IenW.
ISO, 2007. ISO 10456 Building Materials and Products - Hydrothermal Properties - Tabulated Design Values and Procedures for Determining Declared and Desgin Thermal Values. ISO.
Kinnunen, P., Yliniemi, J., Talling, B., Illikainen, M., 2016. Rockwool waste in fly ash geopolymer composites. J. Mater. Cycles Waste Manag. 19, 1220–1227. https://doi.org/10.1007/s10163-016-0514-z.
Kizinievič, O., Balkevičius, V., Pranckevičienė, J., Kizinievič, V., 2014. Investigation of the usage of centrifuging waste of mineral wool melt (CMWW), contaminated with phenol and formaldehyde, in manufacturing of ceramic products. Waste Management 34 (8), 1488–1494. https://doi.org/10.1016/j.wasman.2014.01.010.
Klima, K.M., Luo, Y., Brouwers, H.J.H., Yu, Q., 2023. Effects of mineral wool waste in alkali activated-artificial aggregates for high-temperature applications. Construct. Build. Mater. 401, 132937 https://doi.org/10.1016/j.conbuildmat.2023.132937.
Koh, C.H., Schollbach, K., Gauvin, F., Brouwers, H.J.H., 2022. Aerogel composite for cavity wall rehabilitation in The Netherlands: material characterization and thermal comfort assessment. Build. Environ. 224, 109535 https://doi.org/10.1016/j.buildenv.2022.109535.
Koh, C.H., Luo, Y., Gauvin, F., Schollbach, K., 2024. Utilization of geopolymer in wood wool insulation boards: design optimization, development and performance characteristics. Resour. Conserv. Recycl. 204, 107510 https://doi.org/10.1016/j.resconrec.2024.107510.
Kurnitski, J., 2000. Crawl space air change, heat and moisture behaviour. Energy Build. 32 (1), 19–39. https://doi.org/10.1016/S0378-7788(99)00021-3.
Kurnitski, J., Matilainen, M., 2000. Moisture conditions of outdoor air-ventilated crawl spaces in apartment buildings in a cold climate. Energy Build. 33 (1) https://doi.org/10.1016/S0378-7788(00)00061-X.
López-García, A.B., Uceda-Rodríguez, M., León-Gutiérrez, S., Cobo-Ceacero, C.J., Moreno-Maroto, J.M., 2022. Eco-efficient transformation of mineral wool wastes into lightweight aggregates at low firing temperature and associated environmental assessment. Construct. Build. Mater. 345, 128294 https://doi.org/10.1016/j.conbuildmat.2022.128294.
Luo, Y., Yu, Q., 2024. Valorization of mineral wool waste in Class F fly ash geopolymer: geopolymerization, macro properties, and high temperature behavior. Cement Concr. Compos. 145, 105318 https://doi.org/10.1016/j.cemconcomp.2023.105318.
Mastali, M., Zahra, A., Hugo, K., Faraz, R., 2021. Utilization of mineral wools in production of alkali activated materials. Construct. Build. Mater. 283, 122790 https://doi.org/10.1016/j.conbuildmat.2021.122790.
Nielsen, E., Nørhede, P., Ladefoged, O., Tobiassen, L., 2013. Evaluation of Health Hazards by Exposure to Mineral Wools (Glass, Stone/slag, HT) and Proposal of a Health-Based Quality Criterion for Ambient Air. The Danish Environmental Protection Agency.
Oliveira, d., Jokipii-Lukkari, K.S., Luukkonen, T., 2024. Assessing alkali activation of waste stone wool from greenhouses combined with direct foaming or granulation to obtain recycled plant substrate. Open Research Europe 4. https://doi.org/10.12688/openreseurope.17101.1.
Pavel, C.C., Blagoeva, D.T., 2018. Competitive Landscape of the EU's Insulation Materials Industry for Energy-Efficient Buildings. Publications Office of the European Union, Luxembourg.
Pavlin, M., Horvat, B., Frankovič, A., Ducman, V., 2021. Mechanical, microstructural and mineralogical evaluation of alkali-activated waste glass and stone wool. Ceram. Int. 47 (11), 15102–15113. https://doi.org/10.1016/j.ceramint.2021.02.068.
Ramírez, C.P., Sánchez, E.A., Merino, M.d.R., Arrebola, C.V., Barriguete, A.V., 2018. Feasibility of the use of mineral wool fibres recovered from CDW for the reinforcement of conglomerates by study of their porosity. Construct. Build. Mater. 191, 460–468. https://doi.org/10.1016/j.conbuildmat.2018.10.026.

Ramírez, C.P., Merino, M.d.R., Arrebola, C.V., Barriguete, A.V., Kosior-Kazberuk, M., 2019. Analysis of the mechanical behaviour of the cement mortars with additives of mineral wool fibres from recycling of CDW. Construct. Build. Mater. 210, 56–62. https://doi.org/10.1016/j.conbuildmat.2019.03.062.

RVO, 2020. Lange termijn renovatiestrategie: op weg naar een CO2-arme gebouwde omgeving (Long-Term renovation strategy: en route to a low-CO2 built environment). In: Rijksdienst Voor Ondernemend Nederland. Den Haag.

RVO, 2021. Marktinformatie isolatiematerialen, isolatieglas en HR-ketels 2010-2020 (Market information on insulation materials, insulating glass and high-efficiency boilers 2010-2020). Rijksdienst Voor Ondernemend Nederland. Den Haag.

Siligardi, C., Miselli, P., Francia, E., Gualtieri, M.L., 2017. Temperature-induced microstructural changes of fiber-reinforced silica aerogel (FRAB) and rock wool thermal insulation materials: a comparative study. Energy Build. 138, 80–87. https://doi.org/10.1016/j.enbuild.2016.12.022.

Väntsi, O., Kärki, T., 2014. Mineral wool waste in Europe: a review of mineral wool waste quantity, quality, and current recycling methods. J. Mater. Cycles Waste Manag. 16, 62–72. https://doi.org/10.1007/s10163-013-0170-5.

Vijay, P.V., Gadde, K.T., GangaRao, H.V.S., 2019. Structural evaluation and rehabilitation of century-old masonry and timber buildings. J. Architect. Eng. 25 (2), 05019001 https://doi.org/10.1061/(ASCE)AE.1943-5568.0000350.

Viljanen, M., Bergman, J., Grabko, S., Xiaoshu, L., Yrjoelae, R., 1999. Ensuring the Long Service Life of Unheated Buildings. Evaluation Methods to Avoid Moisture Damage in Unheated Buildings. Helsinki Univ. of Technology.

WUFI, 2018. WUFI Plus 3.1 Manual.

WUFI Mateial Database, *POROTON-WDF Perlitefüllung*.

Yliniemi, J., Ramaswamy, R., Luukkonen, T., Laitinen, O., Sousa, Á.N.d., Huuhtanen, M., Illikainen, M., 2021. Characterization of mineral wool waste chemical composition, organic resin content and fiber dimensions: aspects for valorization. Waste Management 131, 323–330. https://doi.org/10.1016/j.wasman.2021.06.022.

Zorić, D., Lazar, D., Rudić, O., Radeka, M., Ranogajec, J., Hiršenberger, H., 2012. Thermal conductivity of lightweight aggregate based on coal fly ash. Journal of Thermal Analysis and Calorimetry 110, 489–495. https://doi.org/10.1007/s10973-012-2339-x.